Available online at www.sciencedirect.com
SCIENCE DIRECT
ELSEVIER
Nuclear Instruments and Methods in Physics Research A 511 (2003) 275–281
NUCLEAR INSTRUMENTS & METHODS IN PHYSICS RESEARCH Section A
www.elsevier.com/locate/nima

Issues in Proton Computed Tomography

H.F.-W. Sadrozinski[a,*], V. Bashkirov[b], M. Bruzzi[a,1], L.R. Johnson[a], B. Keeney[a], G. Ross[a], R.W. Schulte[b], A. Seiden[a], K. Shahnazi[b], D.C. Williams[a], L. Zhang[a]

[a] *Santa Cruz Institute for Particle Physics and Center for Origins Studies, University of California Santa Cruz, Santa Cruz, CA 95064, USA*

[b] *Loma Linda University Medical Center, Loma Linda, CA 92354, USA*

Abstract

We report progress on a feasibility study of Proton Computed Tomography and Proton Transmission Radiography for applications in treatment planning and patient positioning for proton radiation therapy. We analyzed data from proton transmission studies through a hollow aluminum cylinder taken with a telescope of silicon detectors with very high spatial and good energy resolution. In addition, we explored the usefulness of applying a cut on the angular divergence of the transmitted beam in a GEANT4 simulation study.

PACS: 87.53.Tf; 87.53.Vb; 29.40.Wk

Keywords: Proton Computed Tomography; Silicon detectors; GEANT

1. Introduction

X-ray Computed Tomography (XCT) is commonly used to image patients for treatment planning of both photon and proton radiation therapy. The principle of XCT is shown in Fig. 1: a fan or cone photon beam from an X-ray tube traverses the patient and is recorded in a fine-grained detector. The transmitted X-ray intensity depends on the differential attenuation of the transmitted photons, which is related to the atomic number Z and the density of the tissue traversed. By rotating the device around the patient, stacked 2D maps of linear X-ray attenuation are generated, representing a faithful reconstruction of the patient's anatomy.

Proton radiation therapy is a precise form of conformal radiation therapy which employs the favorable depth-dose characteristics of the proton Bragg peak. Avoidance of damage to critical normal tissues and prevention of geographical tumor misses require accurate knowledge of the dose delivered to the patient and verification of the correct patient position with respect to the proton beam. In existing proton treatment centers, dose calculations are performed based on XCT and the patient is positioned with X-ray radiographs,

*Corresponding author. Tel.: +1-831-459-4670; fax: +1-831-459-5777.
E-mail address: hartmut@scipp.ucsc.edu (H.F.-W. Sadrozinski).
[1] Permanent Address: Dipmt. Energetica, Univ. di Firenze, Florence, Italy.

0168-9002/03/$ - see front matter
doi:10.1016/S0168-9002(03)01806-0

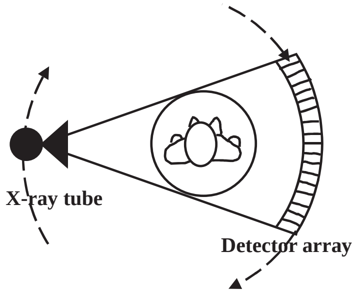

Fig. 1. Schematic view of an XCT set-up. The attenuation of the X-rays in the patient is measured in the detector. Rotation of the apparatus around the patient allows to get stacked two-dimensional pictures of the Z-distribution. In Proton Computed Tomography, the X-ray tube would be replaced by a proton accelerator.

which requires the installation of an X-ray source in the treatment beam line [1].

However, the use of XCT images for proton treatment planning ignores fundamental differences in physical interaction processes between photons and protons and is, therefore, potentially inaccurate. Furthermore, X-ray radiographs mainly depict a patients' skeletal structures and rarely show the tumor itself. Ideally, one would image the patient directly with protons, for example, by measuring their energy loss after traversing the patient [2]. This method has the potential to significantly improve the accuracy of proton radiation therapy treatment planning and the alignment of the target volume with the proton beam.

We recently have begun to investigate the feasibility of Proton Computed Tomography (PCT) and Proton Transmission Radiography (PTR) for treatment planning and patient positioning for proton therapy. In this paper, we will briefly review the basic differences between X-ray and proton imaging and the benefits of protons in cancer treatment. We then describe our present experimental set-up based on a telescope of silicon detectors to explore the feasibility of PCT, followed by a discussion of the data obtained with PTR of a simple object and a comparison with the results of Monte Carlo (MC) simulations, focusing on the usefulness of the angular information of the outgoing proton.

2. Interaction in matter: X-rays vs. proton

Diagnostic and therapeutic X-rays in the energy range of 30–150 keV interact with the imaging object mainly through the attenuation of the photons flux through Compton scattering. The process is statistical in nature, and one measures the number of transmitted photons. After passing through a thickness l, the original number of photons is reduced exponentially to the average number $N(l)$

$$N(l) = N_0 e^{-\mu l} \tag{1}$$

where μ is the attenuation coefficient. Fig. 2a shows the attenuation coefficient [3] as a function

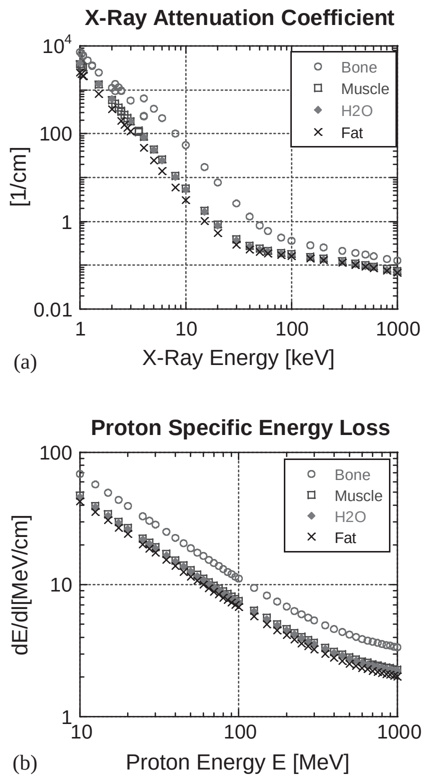

Fig. 2. (a) X-ray attenuation coefficient and (b) proton specific energy loss as a function of energy for bone, muscle, water and fat. The large contrast for bone in X-rays is due to factor 10 times larger attenuation coefficient with respect to water, while the difference between different tissue and water is relatively small both in X-rays and protons. The energy dependence of the specific energy loss can be employed to measure the particle energy.

of energy in the X-ray range of relevance for medical imaging (1–100 keV) for bone, water, muscle, and fat. The energy dependence is very large, but with the exception of bone due to the higher atomic number of calcium, the values of μ are very similar for the different types of tissue. This is the reason why X-ray images of soft tissue are of low contrast, while bone can be imaged very well. It should also be pointed out that in an uniform medium, the largest number of X-rays is absorbed at the entrance of the beams, so that the dose will be highest at the entrance, with an ever decreasing dose extending far into the medium.

Protons with energies used in therapeutic applications (70–250 MeV) lose energy mainly through inelastic collisions with atomic electrons as described by the Bethe–Bloch equation [4]. The energy loss ΔE is the integral over the specific energy loss $\mathrm{d}E/\mathrm{d}l$ over the track length l

$$\Delta E = \int \frac{\mathrm{d}E}{\mathrm{d}l}\,\mathrm{d}l = \int \frac{\mathrm{d}E}{\mathrm{d}x}\,\mathrm{d}x \approx \sum \rho_i \left(\frac{\mathrm{d}E}{\mathrm{d}x}\right)_i \Delta l \qquad (2)$$

where $\mathrm{d}E/\mathrm{d}x$ is the stopping power,[2] i.e., the energy loss per unit density-weighted track length $x = \rho l$, which exhibits only a weak dependence on material traversed, i.e. $\mathrm{d}E/\mathrm{d}x \sim Z/A$ [5].

As indicated in Eq. (2), a measurement of energy loss is essentially a measurement of the density distribution of the tranversed material. Fig. 2b shows the specific energy loss for protons for the same tissues as in Fig. 2a [3]. The energy dependence is fairly strong in the energy range of 50–200 MeV (as exploited by our experiment), but the energy loss difference between different tissues is small due to the small difference in densities. For example, relative to water, bone has $\Delta\rho = 0.5\ \mathrm{g/cm^2}$, and the density difference between fat and muscle is about $\Delta\rho = 0.1\ \mathrm{g\ cm^2}$. Thus proton CT of the human body is inherently low contrast.

Protons undergo multiple Coulomb scattering (MCS) while traversing the material. The projected scattering angle Θ_{MCS} is energy and material dependent [5]:

$$\theta_{\mathrm{MCS}} \approx \frac{13.6\ \mathrm{MeV}}{\beta p} z \sqrt{l/X_0} \qquad (3)$$

where z is the charge of the projectile ($z = 1$ for protons) and X_0 is the radiation length, a material constant characterizing the electromagnetic interaction in matter. For a 250 MeV proton traversing 20 cm of water the multiple-scattering angle is about $\Theta_{\mathrm{MCS}} \approx 1^\circ$.

The basic tissue interactions leave the proton intact (unless it undergoes nuclear interaction), and the properties of individual particles, i.e., energy and exit angle, can be measured and used to reconstruct the energy loss or density distribution of the traversed tissue. This information can then be employed for calculation of proton dose distributions which should be more accurate compared those based on XCT. We have started a program [6] to investigate the feasibility of PCT in support of proton therapy with initial results given in Ref. [7].

3. Advantages of proton therapy

The negative slope of the energy loss curves for protons shown in Fig. 2b has important implications for the application of protons in therapy. While traversing the medium, the protons slow down, and thus their $\mathrm{d}E/\mathrm{d}l$ increases. This is illustrated in Fig. 3 where the particle energy and

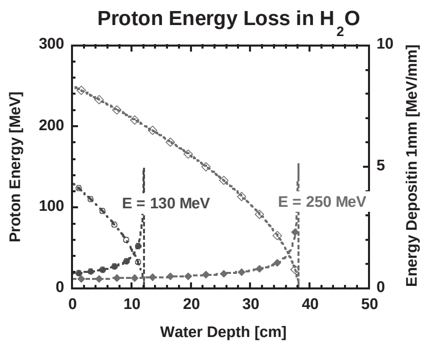

Fig. 3. Proton energy loss in water as a function of depth for two incident proton energies (without energy-range straggling). The open symbols indicate the energy of the protons, and closed symbols the energy deposited in 1 mm water.

[2] The words stopping power and energy loss seem to be used interchangeably in the medical and particle physics community. We are using here the convention of Ref. [5].

the energy loss ΔE in 1 mm path length are plotted vs. the proton path length in water. The energy deposit is characterized by an entrance plateau, at the end of which lies the so-called Bragg peak, where the protons loose a large amount of their residual energy over a small distance. Proton beam treatment makes use of the Bragg peak to deliver maximum dose to the tumor. Beyond the well-defined range the intensity exhibits a rapid distal fall off. For larger tumors, the energy of the proton beam is modulated to vary the range across the tumor.

Proton CT can use the energy loss of protons in the plateau, and thus minimize the dose to the patient. In comparison, X-rays have a high entrance dose, moderate dose at depth, and always contribute dose beyond the target area. Owing to the obvious clinical advantages of proton therapy, there is an increasing number of proton accelerators dedicated to therapy as described in Ref. [8].

4. Experimental setup for PCT study

Our approach in the preliminary PRT and PCT studies [6,7] is based on state-of-the-art silicon strip detectors (SSDs) which measure the energy and position of individual protons. The SSDs provide information on the position of the particle track from the strip number traversed and information on the particles energy from the measurement of the energy deposited in each detector. This system, described in greater detail in Refs. [9,10], permits measurements of the proton position to about 50 μm and determination of the energy of protons in the 20–300 MeV range. The proton energy is derived from the specific energy deposition in each SSD using the time over threshold (TOT) signal as described in Refs. [11,12]. The energy measurement is possible due to the relative steep energy dependence of the stopping power (Fig. 2b).

The SSDs, manufactured by Hamamatsu Photonics HPK, and the readout ASICs used for our experiment, were originally developed for the Gamma-Ray Large Area Space Telescope (GLAST) [11]. The single-sided, AC coupled p-on-n detectors are manufactured from high-resistivity wafers of 400 μm thickness, with a pitch of 194 μm, and outer dimensions of 6.4 cm $\times$ 6.4 cm.

The setup for our initial experiment, described in detail in Ref. [7], was installed on the research beam line of the medical proton synchrotron at Loma Línda University Medical Center [1]. A monochromatic 250 MeV proton beam was degraded by a 25.4-cm-thick (approximately cube-shaped) wax block ($\rho = 0.926\ \mathrm{g/cm^2}$) to a mean energy of about 130 MeV. At a distance of 25 cm downstream from the wax block, the beam encountered the image object, a 5.0-cm-long hollow aluminum cylinder ($\rho = 2.7\ \mathrm{g/cm^2}$) of outer diameter OD = 3.0 cm and inner diameter ID = 0.68 cm. Behind the object, protons were individually detected by two silicon detector modules, each consisting of a pair of single-sided SSDs with strips oriented at right angle to each other. These detectors, located immediately behind and 27 cm downstream of the object, served to measure the spatial coordinates (x and y), the exit angles, and the energy of the protons that either passed by or traversed the object.

5. Energy measurement

A low-noise, low-power, front-end ASIC, the GLAST Tracker Front End (GTFE), developed for the GLAST mission, is used for the readout of the fast silicon detector signals [12]. The GTFE is a binary chip with a threshold settable individually for every channel and a fast output of the TOT, which is used for energy measurement. Self-triggering is accomplished through an OR of the TOT of all channels on one detector. The GTRC allows digitization of the TOT, yielding a measurement of the input charge via the pulse width, i.e., the TOT signal, over a large dynamic range. The electronic calibration of the ASICs demonstrated a linear dependence of the TOT on the charge input up to a duration of 100 μs, at which point the TOT saturates. This translates into valuable energy measurements up to an input charge of 100 fC which corresponds to the average charge deposited by 17 MeV protons in 400-μm-thick Si. We have tested the energy measurement performance of the SSD-TOT system with proton beams of energies between 5 and 250 MeV and recorded the TOT spectra [9,10]. Using the expected and experimentally confirmed TOT vs. energy curve, we find that the energy resolution σ_E/E below 40 MeV is on the order of 15% and increases to about 25% at 250 MeV.

6. Experimental results

The experimental program of our PCT investigation is outlined in Refs. [6,7]. Here we describe a simple PTR experiment. The event data collected in our experiment was comprised of x- and y- hit positions and TOT values from the four silicon planes. Proton transmission images were calculated for each SSD module by averaging the proton energy over a large number ($\sim 10^6$) of individual events, and displayed as 2D maps of proton energy versus the x- and y-strip positions in the respective SSD module. It was found that the image measured with the downstream module (SSD planes 3 and 4) showed almost no object features. This can be explained by the effect of multiple scattering (see Section 5). The two-dimensional plot in Fig. 4 shows the spatial distribution of average energy in the upstream module for proton energies averaged in four by four strip pixels (approximately 0.8×0.8 mm^2), after the proton energy averaged over pixels of 4×4 strips (pixel size approximately 0.8×0.8 mm^2). The image of the phantom projection is clearly seen in the spatial energy distribution.

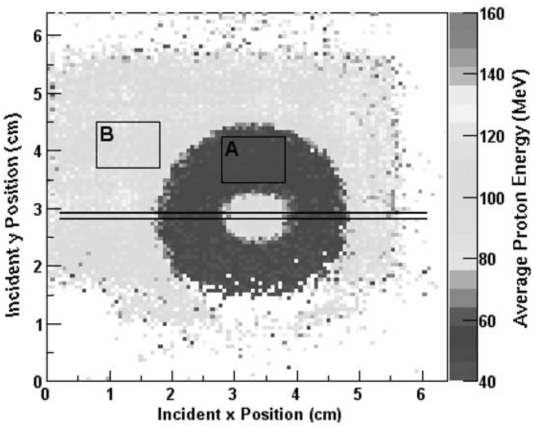

Fig. 4. Spatial distribution of the average energy of protons hitting all four SSD planes. The average energy is projected onto the SSD plane after averaging over pixels of four by four strips. The image of the object can be clearly seen. The horizontal lines indicate the approximate location of the slice of Fig. 6. Areas A and B are selected to evaluate the GEANT4 simulation of Fig. 5.

Note that the coloring of the structure in Fig. 4 is directly proportional to the energy loss in the aluminum object and thus is proportional to the product of its length and density. Fig. 4 thus demonstrates the principle of image formation based on the spatial measurement of proton energy loss behind the image object. Future work will be devoted to improve the accuracy and range of the energy loss measurements.

We further analyzed the transmission image of Fig. 4 by selecting a 4 y-strip wide "slice" through the center of the cylinder ($139 \leqslant y \leqslant 142$ as indicated in Fig. 4), containing pixels of 2×4 strips. Depending on their location, the number of proton events per pixel varied between 100 and 500 protons, owing to the non-uniformity of the beam used in these experiments. The image is characterized by the following attributes:

- The observed energy profile agrees well with the borders of the object.
- The mean energy of the protons inside the central hole of the object is lower than that of protons outside the object.
- The edges of the energy profile of the object appear "fuzzy", i.e., not parallel to the beam, over a distance of several millimeters.

7. GEANT4 simulations

To better understand the features of the proton transmission images presented in Section 6, we performed simulations with the GEANT4 MC toolkit [13]. The GEANT4 code has proved its ability to faithfully simulate the interaction of protons down to low energy [14]. Here, the code was used to define cuts on the data to optimize spatial resolution and contrast of the proton images. Details of the simulations are given in Ref. [15].

Fig. 5 shows the measured and simulated angular distributions of protons in two image areas shown in Fig. 4: area A contains only protons, which traverse the object in its entirety, while area B contains protons which miss the object completely. The difference between the distributions is caused by the increased multiple Coulomb scattering in the object (see Eq. (3)). The agreement between data (symbols) and simulations (histograms) is good in both areas, and indicates that the simulations can be used further to explore the usefulness of angular cuts.

An example angular cut is to discard protons that travel at an angle of more than 0.025 (about 1.5°) with respect to the beam direction. This eliminates about 50% of all protons passing through the object.

The simulated energy profiles in the x and y silicon planes close to the object with and without this cut are shown in Fig. 6a. The location of the profiles is indicated by the horizontal lines

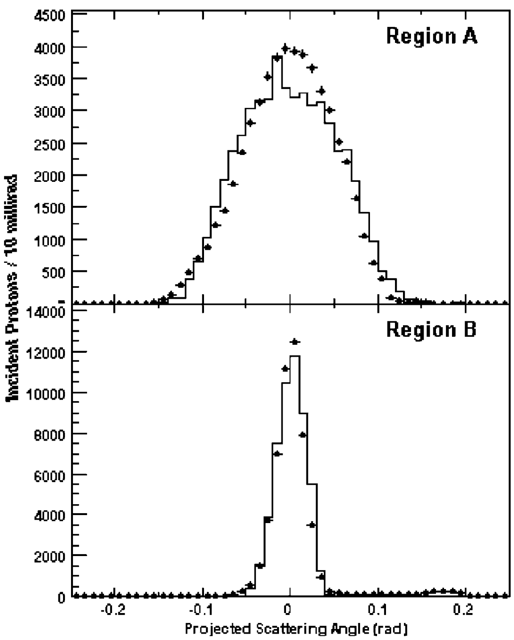

Fig. 5. Comparison between experimental angular distributions (points) and GEANT4 simulations (histograms) in areas A (through object) and B (wax degrader only) of Fig. 4.

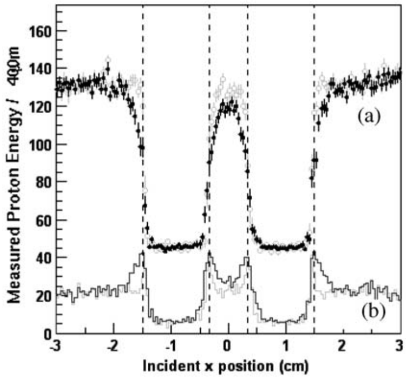

Fig. 6. (a) (Upper half of illustration) MC simulation of the average energy profile of the first SSD module in a 400-μm-wide slice through the center of the object as indicated in Fig. 4. The dashed vertical lines indicate the relative position of the object with respect to the SSD plane. (b) (Lower half) RMS deviation of the proton energy. Note the increase in the RMS at the interfaces between object and air.

(“slice”) in Fig. 4. The simulated energy profiles agree well with the outline of the object (and with the measured energy profile, not shown here, within the limits of the calibration). The mean simulated energy of protons transmitted through the hole is about 10% lower than that for protons passing outside the object. Furthermore, in agreement with the measured energy profile, both the inner and outer walls of the object appear fuzzy.

These image features can be explained by “migration” of protons from the object into the surrounding space due to multiple Coulomb scattering. This assumption is supported by the distribution of the energy spread (RMS), shown in Fig. 6b, which is larger at the interfaces between the object and the surrounding air, indicating a mixture of protons with and without energy loss in this region.

The closed symbols and the red histogram are for all particles, and the open circles and the green histogram are for protons within the angular cut. The improvement in image sharpness is seen in the more vertical interfaces, filling in the hole, and the reduction of the width of the region with increased energy RMS at the interface between object and air.

Applying the angular cut removes most of the migrating protons and, therefore, sharpens the image considerably (Fig. 6a). The transition from Al to air takes place almost within one bin of 400 μm. In addition, the central hole is filling in. The energy RMS plot (Fig. 6b) indicates that the angular cut limits the increased energy spread to just one bin, otherwise, it is nearly constant across the region with the Al object and air, respectively.

8. Conclusions

The exploratory data in this study demonstrate that imaging with protons based on energy-loss measurement in silicon is possible. In addition, the simulations using the GEANT4 toolkit describe the features of the images well, e.g., the influence of multiple scattering and proton migration on the energy and position resolution. Using the simulation tool, we have shown that it is possible to reduce the deleterious image effects of multiple scattering and beam divergence by measuring the exit angles of individual protons with a silicon telescope and applying appropriate cuts.

Acknowledgements

This work was supported by Calspace and the National Medical Technology Testbed Inc. (NMTB) under the US Department of the Army Medical Research Acquisition Activity, Cooperative Agreement DAMD17-972-7016. The views and conclusions contained in this presentation are those of the authors and do not necessarily reflect the position or the policy of the US Army or NMTB.

References

[1] J.M. Slater, J.O. Archambeau, D.W. Miller, M.I. Notarus, W. Preston, J.D. Slater, Int. J. Radiat Oncol. Biol. Phys. 22 (1992) 383.
[2] U. Schneider, E. Pedroni, Med. Phys. 22 (1995) 353.
[3] National Institute for Standards and Technology, PSTAR database, http://physics.nist.gov/PhysRefData/Star/Text/PSTAR.html.
[4] H. Bichsel, Passage of charged particles through matter, American Institute of Physics Handbook, McGraw-Hill, Vol. 42, New York, 1972, pp. 8–189.
[5] D.E. Groom (Ed.), Eur. Phys. J. C15 (2000).
[6] H.F.-W. Sadrozinski, Toward proton CT, 2002 IEEE NSS/MIC in Norfolk, VA, November 2002, SCIPP 02/36.
[7] L.R. Johnson, et al., Initial studies from on proton CT using a silicon strip detector telescope, RESMDD02, Florence, Italy, July 2002, SCIPP 02/32.
[8] S. Peggs, Proton Therapy Accelerators, 2002 IEEE NSS/MIC in Norfolk, VA, November, 2002.
[9] B. Keeney, V. Bashkirov, R.P. Johnson, W. Kroeger, H. Ohyama, et al., A silicon telescope for applications in nanodosimetry, IEEE Trans. Nucl. Sci. NS-49 (2002) 1724.
[10] B. Keeney, A silicon telescope for applications in nanodosimetry, UC Santa Cruz Physics Senior Thesis, 2002, SCIPP 02/16.
[11] E. do Couto e Silva, G. Godfrey, P. Anthony, R. Arnold, H. Arrighi, et al., Nucl. Instr. and Meth. A 474 (1) (2001) 19.
[12] R.P. Johnson, P. Poplevin, H.F.-W. Sadrozinski, E. Spencer, IEEE Trans. Nucl. Sci. NS-45 (1998) 927.
[13] S. Agostinelli, et al., Geant4—A Simulation Toolkit, SLAC-PUB-9350, Nucl. Instr. and Meth. A 506 (2003) 250.
[14] GEANT4 Workshop at SLAC February 18–22, 2002.
[15] L.R. Johnson, et al., Monte Carlo studies of proton CT using a silicon strip detector telescope, 2002 IEEE NSS/MIC in Norfolk, VA, November 2002, SCIPP 02/35.